Macromolecules

ARTICLE

pubs.acs.org/Macromolecules

Morphologies of Linear Triblock Copolymers from Monte Carlo Simulations

Umang Nagpal,[†] François A. Detcheverry,[‡] Paul F. Nealey,[†] and Juan J. de Pablo*[,†]

[†]Department of Chemical and Biological Engineering, University of Wisconsin—Madison, Madison, Wisconsin, 53706-1691, USA

[‡]LPMCN, Université Lyon 1 and CNRS, UMR 5586, F-69622 Villeurbanne, France

ABSTRACT: Recent developments in block copolymer lithography suggest that triblock copolymers could enable fabrication of ultrasmall features over large areas. While the majority of past work with block copolymers has focused on diblocks, triblocks and multiblocks in general could offer distinct advantages for sublithographic patterning. In order to guide selection of appropriate materials and strategies, it is important to first determine the phase behavior that distinct molecular architectures exhibit in the bulk. Theoretically informed Monte Carlo simulations of a coarse grain model are used to predict the bulk morphologies of several linear triblock copolymers in three dimensions. Some of these triblocks are representative of the styrene−isoprene−methyl methacrylate system. The morphologies predicted by simulations, which incorporate fluctuation effects, are compared to those predicted by self-consistent field theory (SCFT). While the two approaches predict similar morphologies, some differences are identified when some of the blocks are short. We then consider several morphologies of lamellae forming triblock copolymer thin films on a patterned substrate, and use free energy calculations to determine the equilibrium states.

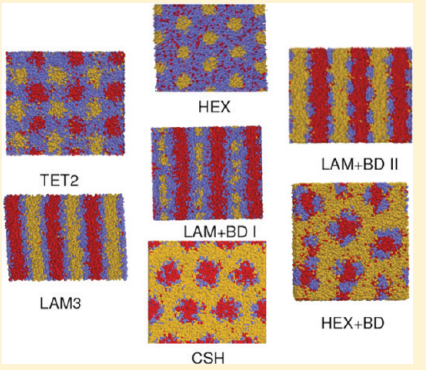

I. INTRODUCTION

Lithographic patterning at sub-50-nm dimensions faces a number of significant challenges. New patterning strategies and materials are needed to meet those challenges. Over the last several years, block copolymer lithography has emerged as a viable approach for patterning small features with nanometer control over large areas. Block copolymer materials self-assemble into ordered structures (or morphologies) with typical periodicity in the 10−50 nm range.[1,2] The spontaneous self-assembly of such morphologies on uniform and patterned substrates has been exploited to produce dense and highly ordered nanostructures for a variety of applications, including quantum dots, flash memory devices, semiconductor capacitors, photonic crystals, magnetic storage media, and nanopores.[1,3−15]

Triblock and multiblock copolymers are particularly important in the context of lithography because they could serve as natural enablers of the concepts of sublithographic patterning and density multiplication.[13] In block copolymer lithography, the assembly of a block copolymer thin film is guided by information (patterns) encoded onto a substrate, either in the form of topography or in the form of chemical patterns. The idea of sublithographic patterning and density multiplication is that only relatively coarse features need to be patterned on a substrate;[12,16,17] the copolymer can then add information to the process in the form of small domains that can be subsequently etched on the underlying surface.

At a coarse-grain level, a melt of AB diblock copolymers can be characterized by two parameters: the product of the Flory−Huggins parameter and molecular weight ($\chi_{AB}N$), and the volume fraction of the A block (f_A). This two-dimensional parameter space has been explored extensively, both experimentally[18−21] and theoretically.[2,22,23] It is now known that only a relatively small set of morphologies can be created by diblock copolymers. These include lamellar, cylindrical, spherical, and gyroid morphologies. Much less is known about the nature and variety of morphologies that arise in multiblock copolymers. For the simplest case, a linear ABC triblock, at least five parameters ($\chi_{AB}N$, $\chi_{BC}N$, $\chi_{CA}N$, f_A, and f_B) are necessary to define the morphology of the material. The corresponding parameter space remains to be fully explored, particularly in the context of thin films and patterned substrates.

Several systems have been considered at the experimental level. A review by Abetz et al.[24] has summarized some of the bulk morphologies that have been observed to date. Of note is the observation that linear ABC triblocks lead to a number of morphologies that do not arise in diblocks. Breiner et al.,[25,26] for example, obtained cylinder-in-cylinder (or core shell), helical, and decorated morphologies. In the latter case, the A block was found to form large domains in a matrix of C block, and the B block was seen to form smaller domains located at the A/C interface. Other morphologies include cylinders on cylinders, spheres on cylinders and spheres on spheres. In different work, Epps et al.[27−29] reported the existence of several continuous network phases, including a core−shell double gyroid, an orthorhombic network, and an alternating gyroid morphology.

Received: February 15, 2011
Revised: May 23, 2011
Published: June 14, 2011

The morphology of triblock copolymers has also been been examined using theory and simulations. Monte Carlo (MC) simulations of lattice models have been used to explore triblock self-assembly in the bulk and under confinement.[30−34] Such calculations, however, have been limited to small system sizes.[35,36] An off-lattice approach, which relied on minimization of the free energy functional, was introduced by Bohbot−Raviv et al.[37] and identified a variety of complex morphologies, including the so-called knitting patterns that can be expected from triblocks. Dynamic density functional theory (DDFT) has also been used to predict the phase behavior of a confined ABA triblock[21]

Several groups have used self-consistent field theory (SCFT) to generate phase diagrams for triblocks. In particular, Tang et al.[38,39] considered linear and star copolymers; these authors identified seven morphologies for the former and nine for the latter. Ye et al. examined the phase behavior of H-shaped ABC block copolymers[40] and π shaped triblock copolymers.[41] Octagon−octagon−tetragon (OOT), three-color hexagonal honeycomb (HEX3), and dodecagon−hexagon−tetragon (DOHT) morphologies were identified by these authors. Recent work by Guo et al.[42] adopted SCFT and a Fourier-space approach to predict a number of new phases for linear ABC triblocks, including a 2-dimensional knitting pattern (KP) and a 3-dimensional gyroid with spheres. However, due to computational limitations, their studies were restricted to $\chi_{CA} \ll \chi_{AB} \approx \chi_{BC}$. Sun et al.[43] used real-space SCFT in three dimensions to investigate linear triblocks and found intrinsically three-dimensional structures such as perforated lamellae and network phases. Their calculations were limited to $f_A = f_C$.

As useful and informative as past SCFT calculations have been, they have generally been limited to two-dimensional systems and, perhaps more importantly, they have not considered the effects of fluctuations in the resulting phase diagrams. Some of the morphologies observed in experiments, including helical, cylinders on cylinders, perforated cylinder in cylinder, spheres on cylinder, and spheres on spheres,[25,26] have not been predicted by SCFT. It is therefore of interest to determine whether such morphologies can be predicted or not by theoretical means, particularly through the use of approaches that enable consideration of large systems in three dimensions and thermal fluctuations.

In this work, we use Monte Carlo simulations of the standard model of block copolymers[44−47] to predict the morphologies of linear ABC triblock copolymers. Our calculations are fully three-dimensional and incorporate the effects of fluctuations.[48,45] We generate phase diagrams for these triblocks as a function of composition. Our results are compared to those obtained by earlier SCFT-based studies[38,39] of the same systems. We then consider thin films of triblocks on nanopatterned substrates and focus on lamellar morphologies that could be particularly useful for lithographic applications. In cases where simulations reveal competing morphologies, we identify the equilibrium state through free energy calculations that rely on thermodynamic integration.

II. METHOD

Model. We consider n AB block copolymer molecules confined in a volume V at temperature T. Each chain contour is discretized with N beads. A vector $\mathbf{r}_i(s)$ denotes the position of the sth bead in the ith chain. The Hamiltonian $\mathscr{H}$ includes bonded (b) and nonbonded (nb) contributions to the energy:

$$\mathscr{H}[\{\mathbf{r}_i(s)\}] = \mathscr{H}_b[\{\mathbf{r}_i(s)\}] + \mathscr{H}_{nb}[\varphi_A, \varphi_B, \varphi_C] \quad (1)$$

Bonded interactions are described by harmonic springs between adjacent beads on the chains

$$\frac{\mathscr{H}_b[\mathbf{r}_i(s)]}{k_B T} = \frac{3}{2}\sum_{i=1}^{n}\sum_{s=1}^{N-1}\frac{[\mathbf{r}_i(s+1) - \mathbf{r}_i(s)]^2}{b^2} \quad (2)$$

where k_B is the Boltzmann constant, $b^2 = R_e^2/(N-1)$ is the mean squared bond length and R_e^2 is the mean-squared end-to-end distance for an ideal chain.

Nonbonded interactions are described by a functional of the local densities $\varphi_A(\mathbf{r})$, $\varphi_B(\mathbf{r})$, and $\varphi_C(\mathbf{r})$, which are determined from the bead positions. Here we adopt a compressible version of the Edwards model.[49] These interactions are of the form

$$\frac{\mathscr{H}_{nb}[\varphi_A, \varphi_B, \varphi_C]}{k_B T} = \rho_o \int_V d\mathbf{r}\left[\chi_{AB}\varphi_A\varphi_B + \chi_{BC}\varphi_B\varphi_C + \chi_{CA}\varphi_C\varphi_A + \frac{\kappa}{2}(1 - \varphi_A - \varphi_B - \varphi_C)^2\right] \quad (3)$$

where ρ_0 is the average bulk number density of beads. The Helfand quadratic approximation[50] is used to restrict the deviation of local density fluctuations from the average value.

In a dense melt, the invariant degree of polymerization $\overline{N}$ is proportional to the molecular weight. The coarse grain parameters used in our model are R_e, which sets the length scale, $\overline{N} = \rho_o R_e^3/N$, which estimates the number of chains a given chain interacts with, κ, which controls density fluctuations, and the set of three Flory−Huggins parameters.

The coarse grain model of eqs 1, 2, and 3 is similar to that generally used in the SCFT method[49] (the compressibility term is often omitted in SCFT treatments). A "particle-to-mesh" (PM) technique[47] is employed to compute the local densities. Here, the simulation domain is divided into a grid with cubic cells in which the number of beads is counted to determine local densities. The grid spacing ΔL is a discretization parameter that defines the interaction range.

Monte Carlo Simulations. Our Monte Carlo (MC) simulations rely on a standard Metropolis sampling algorithm. Trial moves are accepted with probability $p_{acc} = \min[1, \exp(-\Delta H/k_B T)]$, where ΔH denotes the difference in energy between the trial and original configurations. Four MC moves are employed: single displacement, reptation of single or multiple beads, translation of the entire chain, and reversal of the sequence of blocks while keeping the same chain configuration. For faster equilibration, reptation accounts for the largest percentage of moves (90%). Because of the soft nature of PM-based interactions, configurational bias methods are not required for efficient reptation.

Variable Cell Shape. Within the mean-field approximation of the standard model considered here, the internal stress tensor is given by[51]

$$\frac{\sigma_{\alpha\beta}}{k_B T} = -\frac{nN}{V}I_{\alpha\beta} + \frac{3}{V}\sum_{i=1}^{n}\sum_{s=1}^{N-1}\left\langle\frac{(N-1)}{R_e^2}\, b_{i,\alpha}(s) b_{i,\beta}(s)\right\rangle \quad (4)$$

where I is the identity tensor, $\alpha,\beta \in \{x,y,z\}$, $b_i(s) = r_i(s+1) - r_i(s)$ is the bond vector joining two adjacent beads, and $\langle\rangle$ denotes a thermal average. This tensor is used to determine the approximate equilibrium periodicity of a given morphology. For example,

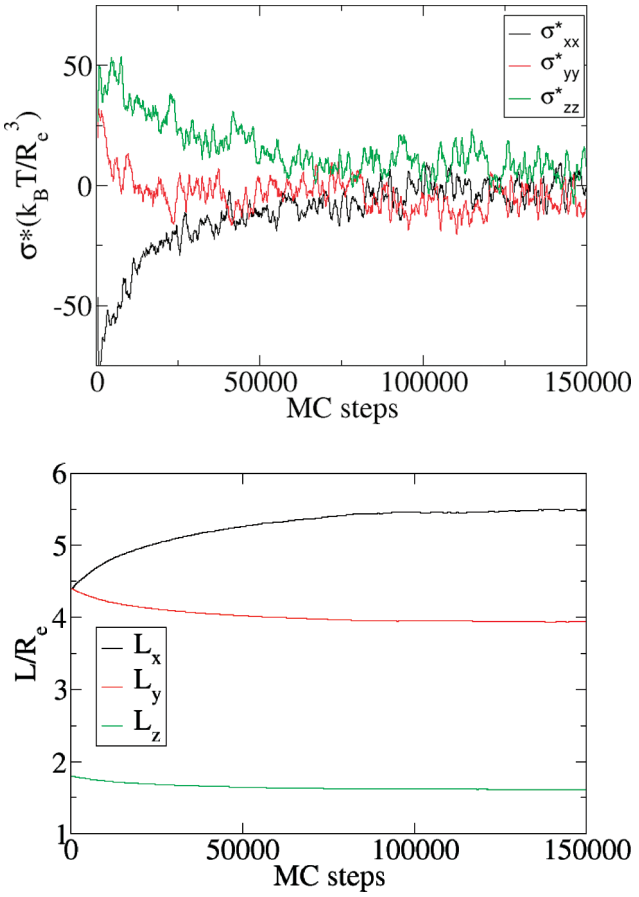

Figure 1. (Top) Stress tensor as a function of MC steps, $\sigma^* = D\sigma$ is the traceless part of the tensor. (Bottom) Box dimensions as a function of MC steps. The parameters of the copolymer are $\chi_{AB}N = \chi_{BC}N = \chi_{CA}N = 55$ and $f_A = f_B = f_C = (1)/(3)$.

for the lamellar morphology, the equilibrium spacing is reached when σ is isotropic. The variable cell-shape method, originally introduced by Bohbot-Raviv and Wang,[37] is used as in previous work.[52,47] A rectangular box with rectangular cells is assumed and vectors h_1,h_2,h_3 constitute the box sides. The matrix concatenating these three vectors $H = [h_1,h_2,h_3]$ evolves in the MC simulation according to

$$\frac{dH}{dt} = -\lambda D\left\langle H^{-1}\Sigma H^{T-1}\right\rangle \qquad (5)$$

where t corresponds to the number of MC moves, and H^{-1} and H^T denote the inverse and transpose of H, respectively. For a matrix A, the operator D is defined as $DA = A - (1)/(3)\mathrm{Tr}(A)I$. While keeping a constant volume, the box dimensions evolves until the isotropic stress condition $\sigma_{xx} = \sigma_{yy} = \sigma_{zz}$ is reached. The parameter λ is used to tune the amplitude of shape changes. Figure 1 illustrates how the stress and box dimensions change until they converge to their equilibrium values. Note that variable cell shapes were only used to obtain bulk morphologies and were not used for thin films.

Parameters. In the following, the invariant degree of polymerization is fixed at $\overline{N} = 128^2$, which is representative of copolymers used in experiments. The compressibility parameter is set to $\kappa N = 50$ (see ref 53 for a discussion of this choice). The chain contour discretization $N = 60$ results from a compromise between computational demands and resolution. On the one hand, small discretization N yields faster computations but, on the other hand, each block must contain a minimum number of beads, thereby requiring a large value of N if one block is short. We have observed, for instance, that using $N = 30$ is not sufficient when $f = 0.1$. In that case the shorter block consists of only three beads, which prevents the formation of certain morphologies (e.g., core−shell) that are actually observed when we go to higher discretizations, e.g., $N = 60$. The grid spacing used in all simulations is $\Delta L = 0.122$, which ensures that each grid cell contains an average of about 14 beads.

Simulations of the bulk system rely on periodic boundary conditions in all directions. The boundary conditions for thin film and patterned substrates are described below. For the bulk case, the initial dimensions of the simulation box are $L_x = L_y = 4.4R_e$, and $L_z = 1.8R_e$, which, in conjunction with the variable cell shape, are large enough to accommodate all morphologies of interest to this work. The initial condition consists of chains placed in a random manner in a simulation box. Equilibration times vary with the morphology, but the order of magnitude is 10^5 MC steps. Multiple realizations were conducted to confirm that the resulting morphologies were equilibrium structures as opposed to metastable morphologies.

It is important to note that the χ parameter introduced in our model and that involved in SCFT are not equal; the former is a "bare" χ parameter, while the latter is an "effective" χ parameter. However, within the present model, we expect the difference between the two to be small. Furthermore, an exact relationship between bare and effective χ, valid for the model under study, is at present not available. For those reasons, in the following, and in the absence of a better alternative, we work under the assumption that our χ parameter and the *SCFT* χ parameter are comparable, but not identical. In cases where simulations and SCFT give rise to different morphologies for a specific value of χ, we explore a range of values above and below our bare χ in order to draw more meaningful comparisons between the two approaches. Additional details on this issue are given in the appendix.

III. RESULTS

A. Bulk Morphologies. Our MC approach has been applied to determine the phase diagram of linear triblock copolymers in the bulk. To compare with results from SCFT calculations by Tang et al.,[38,39] and keeping in mind the caveat mentioned above about bare and effective χ parameters, we chose the same combination of Flory−Huggins parameters, namely χ_{AB}, χ_{BC}, and χ_{CA}. Four distinct sets of parameters are considered, mostly in the intermediate segregation regime; for each of them, a ternary phase diagram that covers the entire copolymer composition range is generated from simulations.

Seven of the nine morphologies observed in our simulations are shown in Figure 2. Note that, in contrast to SCFT, the individual domains exhibit significant variation in size and shape, as clearly visible in the instantaneous configurations shown in that figure. Three morphologies are lamellar in nature: three-phase lamellae (LAM3), and lamellae with "beads", either at the interface (LAM+BD II) or inside one domain (LAM+BD I). Three morphologies have hexagonal symmetry: hexagonal cylinders in a matrix (HEX), hexagonal cylinders with a shell in a matrix (CSH), and hexagonal cylinders with distinct beads, around the cylinders (HEX+BD). The CsCl morphology is reminiscent of the body centered cubic of diblock copolymers,

and the tetragonal arrangement (TET2) can be seen as the analogous structure in two dimensions. Finally, the network/bicontinuous phase consists of a network of core shell domains, with each node connecting three domains. This last morphology is reminiscent of the gyroid phase of diblocks; however, for the system sizes considered here, it proved difficult to ascertain the symmetry of this phase.

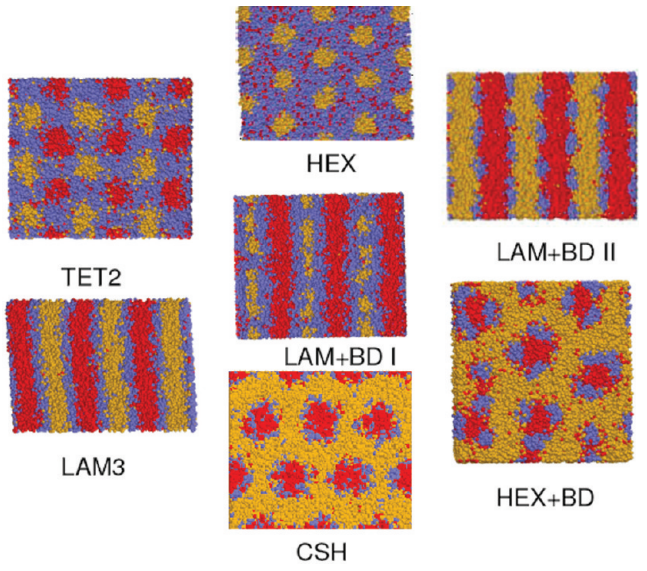

Figure 2. Representative configurations of seven morphologies produced for linear triblocks using MC simulations: lamellar phase (LAM3), hexagonal phase (HEX), core−shell hexagonal phase (CSH), two tetragonal lattices (TET2), lamellar phase with beads inside (LAM+BD I), lamellar phase with beads at the interface (LAM+BD II), hexagonal phase with beads at the interface (HEX+BD).

The first two sets of parameters considered here correspond to the same degree of repulsion between all blocks, with $\chi_{AB}N = \chi_{BC}N = \chi_{CA}N = 35$ or 55. Note that in both cases, the system is then invariant under permutation of A and C blocks. Nonetheless, as a test of equilibration, one simulation (or more) was run for each and every combination of parameters. The corresponding phase diagrams are indeed symmetric and are shown in Figures 3 and 4, along with the SCFT results of refs.[38,39] Most often (32−34 cases out of 36), the two approaches yield the same morphology. A few differences are found, however, for $\chi_{AB}N = \chi_{BC}N = \chi_{CA}N = 35$; they are always located in the corners of the triangle, which implies that at least one block is short and domains are small. For $f_A = f_B = 0.1$, for instance, our MC simulations yield cylindrical domains which contain both A and B beads. SCFT predicts a core shell morphology (CSH), where A and B beads form two distinct domains, a cylindrical core of A surrounded by a shell of B. In order to determine whether this difference is due to a mismatch between the "bare" χ parameter, while the latter is an "effective" χ parameter, we explore the morphology that arises when the bare χ is changed from $\chi N = 30$ to $\chi N = 40$. We find that in that entire range, our simulations continue to predict cylindrical domains that contain A and B beads and that differ from the core−shell morphology of SCFT.

Besides the discrepancy in χ parameters, at least two factors could explain the difference between the MC and SCFT results. First, SCFT formally corresponds to the limit of infinite degree of polymerization ($\overline{N} \to \infty$), where fluctuations become negligible. MC simulations, on the other hand, involve a finite degree of

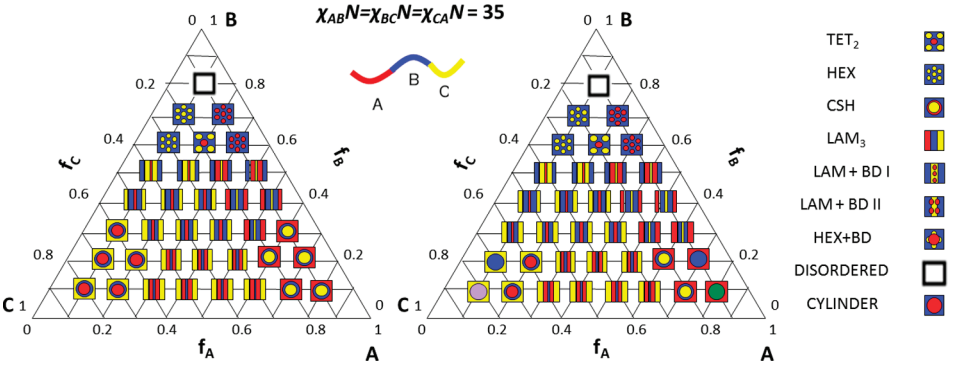

Figure 3. Phase diagram predicted by SCFT (left) and by MC simulations (right).

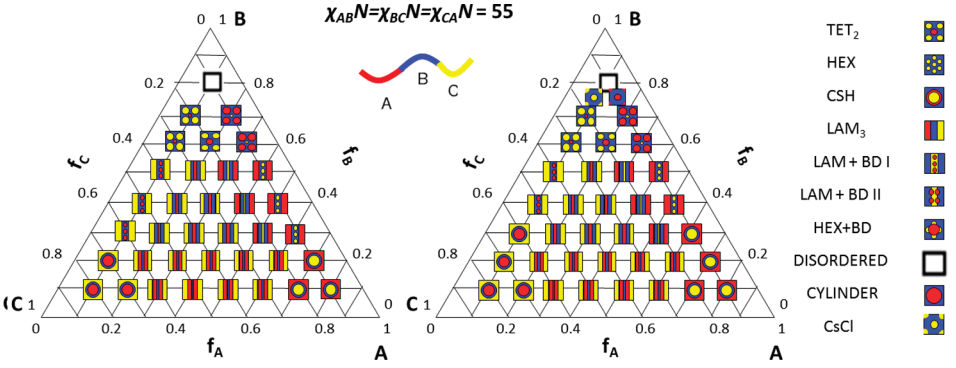

Figure 4. Morphologies predicted by SCFT (left) and by MC simulations (right).

dx.doi.org/10.1021/ma200330f |*Macromolecules* 2011, 44, 5490–5497

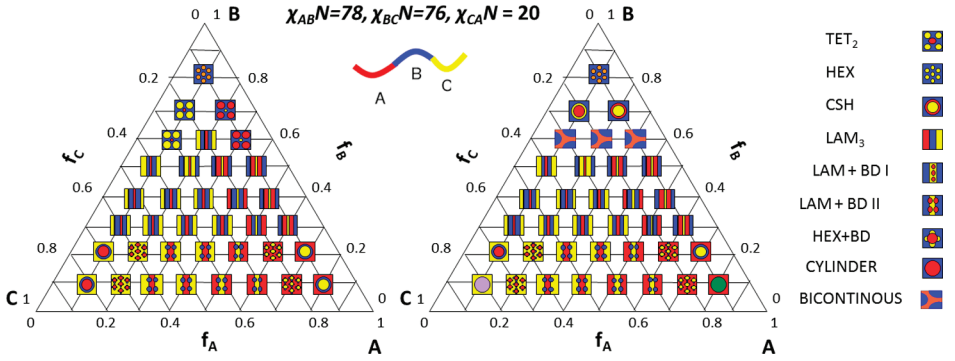

Figure 5. Morphologies predicted by SCFT (left) and by MC simulations (right).

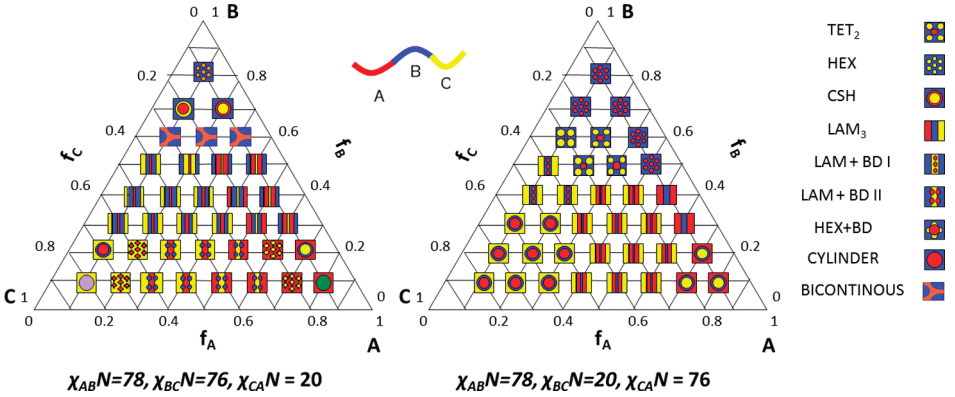

Figure 6. Comparison of phase diagrams predicted by MC simulations.

polymerization (here $\overline{N}$ = 128[2]) and thus include the effect of fluctuations.[63] Second, our melt exhibits a finite compressibility (see ref 53 for details), whereas the SCFT result was obtained for a strictly incompressible melt.[54] In addition to those differences in physical parameters, the finite discretization of our chains could also play a role. For one particular case ($f_A = f_B = 0.1$), we increased the chain discretization to N = 120 and 240, and confirmed that the cylindrical morphology continues to emerge, as opposed to the CSH morphology. Alternatively, while keeping N = 60, the compressibility parameter was increased to 100 and 500, and we observed the same result. These observations suggest that fluctuations (as opposed to finite discretization or compressibility effects) play a central role in determining the equilibrium morphology, particularly when the fraction of two of the components are much lower than that of the third.

The phase diagram for $\chi_{AB}N = \chi_{BC}N = \chi_{CA}N$ = 55 is shown in Figure 4 and turns out to be identical to the one predicted by SCFT. In particular, the core−shell morphology is now found in the corners of the triangle, as predicted by SCFT. In contrast to the previous case, it appears that the repulsion between blocks is large enough to yield a distinct core and shell, even in the presence of fluctuations.

In the process of simulating varying fractions of components, a CsCl morphology was found for $f_A = 0.1, f_B = 0.75$. This structure could not be observed in two-dimensional SCFT calculations, but was considered as a candidate morphology in the theoretical approach of Zheng et al.,[22] and has been observed in experiments.[55]

For the third and fourth phase diagrams, the combinations of parameters considered here correspond to triblocks with blocks

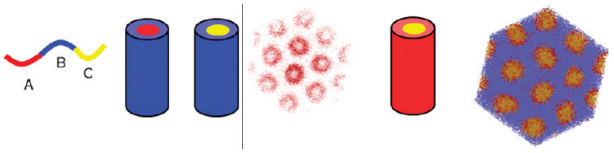

Figure 7. Comparison of core shell (CSH) with end blocks as matrix (left) and CSH with middle block as matrix obtained (right) for $\chi_{AB}N$ = 78,$\chi_{BC}N$ = 76,$\chi_{CA}N$ = 20 and f_A = 0.1, f_B = 0.8 and f_C = 0.1 respectively.

made up of isoprene (I), styrene (S), and methyl methacrylate (M). Figure 5 corresponds to a triblock with block sequence SIM, while Figure 6 corresponds to a sequence ISM. In the former, MC and SCFT predictions differ in two ways. First, the network phase is obtained for f_B = 0.6 and f_A = 0.1, 0.2, 0.3, whereas two-dimensional SCFT calculations yield hexagonal and lamellar morphologies at that composition. Second, for the regions where SCFT predicts hexagonal morphologies (f_B = 0.7, f_A = 0.1, and f_A = 0.2), our simulations predict a core−shell (CSH) morphology, as shown in Figure 7. This CSH morphology includes a matrix consisting of the longest block (B, the middle block), while the end block (A and C) form the core and shell.[64] One possible reason for the formation of this core−shell morphology is that the interaction parameter for the A−C block is much lower than that for the A−B or the B−C block. Hence, A prefers to become the core and C prefers to become the shell and vice versa.

B. Thin Films on Patterned Substrates. A complete characterization of the bulk phase behavior is a necessary first step. However, we are ultimately interested in thin films and their

dx.doi.org/10.1021/ma200330f |*Macromolecules* 2011, 44, 5490–5497

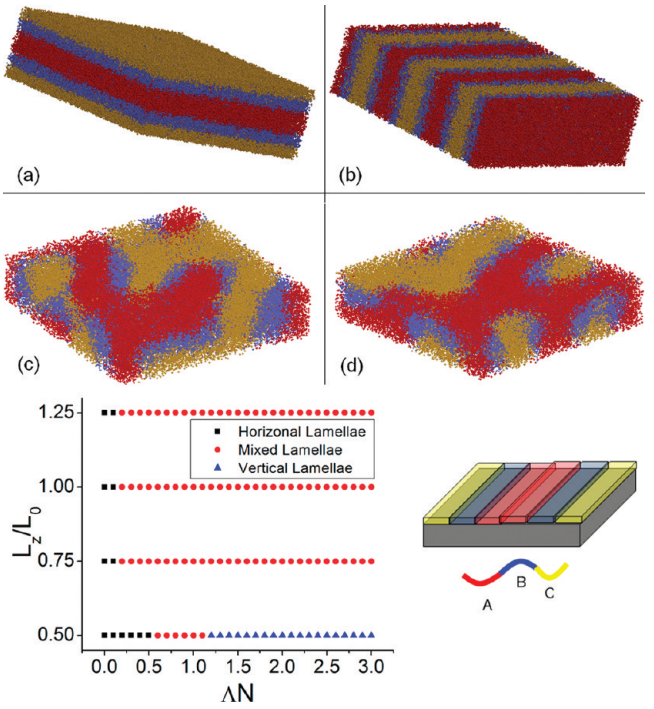

Figure 8. (Top) Horizontal (a), vertical (b), and mixed lamellae (c and d) morphology. (Bottom) Morphologies observed as a function of pattern strength ΛN and film thickness L_z.

applications to nanolithography.[3,11] As in previous work,[11,56] our aim is to guide the assembly of triblock copolymers through the use of nanopatterned substrates. Triblock copolymers could offer significant advantages over diblocks in that interfacial regions would be narrower and process latitude could be broader. Vertical lamellae are particularly interesting in this context, and we seek to identify the conditions leading to this particular morphology. We focus on the influence of film thickness, a parameter that is easily modified in experiments.

The patterned surface is modeled by a potential, U_S, that acts on each bead:

$$\frac{U_S(\mathbf{r},K)}{k_BT} = -\frac{\Lambda_S^K}{d_S/R_e}\exp\left[-\frac{z^2}{2{d_S}^2}\right] \qquad (6)$$

where $\Lambda_S^K N$ determines the strength of interaction between the substrate S and a bead of type $K = A$, B, or C. Patterns considered in the following consist of parallel stripes periodically repeated with periodicity L_S. We consider a three-striped A/B/C pattern, where all stripes have equal width again. The A stripe, indicated by the subscript AS, attracts the A beads and repels B and C beads, with $\Lambda_{AS}^A N = -\Lambda_{AS}^B N = -\Lambda_{AS}^C N = \Lambda N$. Similar parameters hold for a B or C stripe. With regards to the triblock, we set $f_A = f_B = f_C = (1)/(3)$, which yield a lamellar morphology in the bulk for all phase diagrams. We choose a pattern with all the stripes having the same width.

We now examine the changes in morphology that arise when the strength of the pattern interaction and its thickness are varied. Figure 8 summarizes the structures seen for five different realizations and for 30 values of interaction strength. Three kinds of morphologies are observed: they are all lamellar but differ in the domain orientation, which is perpendicular to the substrate, parallel or mixed (see Figure 8). Long simulations performed

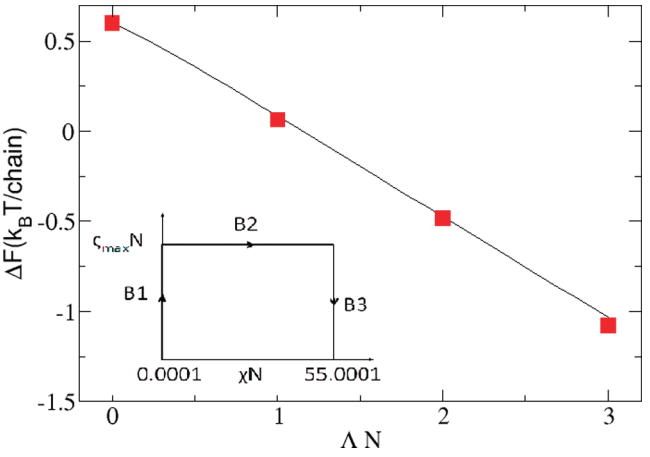

Figure 9. Free energy difference between vertical and horizontal lamellae as a function of pattern strength ($L_z = 0.5L_0$). The points represent the results obtained with the integration path shown in the inset. The line results from integration along increasing ΛN (see text). Inset: The three branches $B1$, $B2$, and $B3$ used to find the free energy difference between the disordered phase at $\chi N = 0$ and the ordered phase at $\chi N = 55$.

for a smaller number of cases suggest that only horizontal and vertical lamellae are stable, equilibrium morphologies. In order to delineate the phase boundary between these two states, we performed free energy calculations for one particular case as outlined below.

The free energy difference between the vertical and horizontal lamellae ($\Delta F = F_\perp - F$) was calculated using thermodynamic integration. The free energy change in going from a morphology α to a morphology β upon changing a parameter u is given by

$$\Delta F_{\alpha\to\beta} = \int_{u_\alpha}^{u_\beta} du\left\langle\frac{\partial\mathscr{H}}{\partial u}\right\rangle \qquad (7)$$

where $\langle\rangle$ denotes a thermodynamic average. The intermediate states between α and β must form a completely reversible path, free of discontinuities or other singularities. To avoid abrupt transitions, an artificial external field was imposed to constrain the system in a desired state.[57] The external field is given by $(U_{ext}(\mathbf{r},K))/(k_BT) = -\zeta N\Sigma_K f_{ext}^K(\mathbf{r},K)$ where ζ is the parameter used to adjust the strength of the field and the corresponding energy is $\mathscr{H}_{ext} = \Sigma_{bead(i)}U_{ext}(\mathbf{r}_i,K_i)$. For a given structure, $f_{ext}(\mathbf{r})$ is defined from the local densities and given by $f_{ext}^K = \langle\varphi_K/(\varphi_A+\varphi_B+\varphi_C)\rangle$ where $K = A$, B, or C.

To evaluate ΔF, we computed both $F_\perp - F_{dis}$ and $F - F_{dis}$, where F_{dis} is the free energy of the disordered phase. The path of thermodynamic integration comprises three branches[57] and is shown schematically in the inset of Figure 9. Starting from the disordered morphology ($\chi_{AB}N = \chi_{BC}N = \chi_{CA}N = 0$), the external field f_{ext} is first increased until its strength reaches its maximal value $\zeta_{max}N$ (branch $B1$). At the maximum strength of the external field, χ_N is increased to its maximum value $\chi_{AB}N = \chi_{BC}N = \chi_{CA}N = 55$ (branch $B2$). The external field f_{ext} is finally turned down to zero at maximum value of χ_N (branch $B3$). Using this process with the vertical and horizontal lamellae, we computed ΔF for $\Lambda N = 0$, 1, 2, and 3; the results are shown with points in Figure 9. A second set of calculations was performed using a simpler integration path: a single "branch" going from $\Lambda N = 0$ to $\Lambda N = 3$. This permits calculation of ΔF as a function of

dx.doi.org/10.1021/ma200330f |*Macromolecules* 2011, 44, 5490–5497

Λ, once a reference point is known.[65] The result is plotted with a line in Figure 9. It shows good agreement with the first calculation, which confirms the accuracy of the method.

Free energy calculations show that the equilibrium morphology for $L_z = 0.5L_0$ consists of horizontal lamellae for $\Lambda N < 0.5$ and vertical lamellae for $\Lambda N > 1.2$. Going back to Figure 8, one can notice that in the interval $0.6 < \Lambda N < 1.2$, the mixed lamellae morphology is the final result of simulations,[66] but not the equilibrium morphology; it is thus metastable. Such metastability has been observed previously with diblocks on incomplete patterns.[17]

IV. CONCLUSION

Theoretically informed Monte Carlo simulations of the standard model of block copolymers[46] were used to investigate the morphology of linear triblock copolymers as a function of composition and interaction strength. This approach allowed us to investigate three-dimensional systems and includes the effects of fluctuations. The phase diagrams obtained with MC simulations are very similar to those found by Tang et al.[38] using SCFT calculations on two-dimensional systems. Note, however, that differences were found in a few cases, particularly when the lengths of some of the blocks (and the sizes of the corresponding domain) were small. We ascribed these differences to the dimensionality or the system and the effects of fluctuations. This observation is of importance in the context of nanolithography, where one seeks to improve or augment lithographic processes by creating the extremely small domains afforded by triblock materials.

Having delineated the bulk phase behavior of the linear copolymers considered here, we proceeded to examine the assembly of lamellar morphologies on striped-patterned substrates. It was shown that a number of new phases can arise. In some cases, it was found that simulations can yield metastable structures that emerge as a result of the morphology formation or dynamic of the assembly process. It was also shown that in such cases precise free energy calculations allow one to distinguish thermodynamically stable from metastable morphologies. These results are relevant in the context of lithography because the number of defects that may arise in a particular situation are closely related to the stability of distinct morphologies and the free energy barriers that exist between them.

Triblock copolymers can adopt a variety of morphologies in the bulk. Yet, as is the case for the diblocks, an even larger set of structures can be anticipated in the presence of a patterned substrate in thin films. Adding the choice of triblock to the choice of a pattern, one is faced with a daunting number of possibilities. Because experimental characterization of unknown morphologies remains a challenge, there is a need for methods that are efficient, even for three-dimensional systems (a necessary condition for lithography with thin films). The methods employed here provide a step in this direction, and warrant additional studies aimed at exploring the full complexity of triblock systems in the context of sublithographic patterning.

■ APPENDIX: BARE AND EFFECTIVE χ PARAMETERS

In this appendix, we discuss the connection between the χ parameters introduced in the SCFT and in our Monte Carlo simulations.

Literature studies[58−60] have pointed out the distinction between the bare χ (χ^b) and the effective χ (χ^e) parameters. The bare χ^b characterizes the interaction at a microscopic level, for instance in an incompressible lattice model, $\chi^b = (z)/(2)(\varepsilon_{AA} + \varepsilon_{BB} - 2\varepsilon_{AB})$, where z is the lattice coordination number and the ε's are the interaction energies; χ^e includes short-range fluctuations and is the true thermodynamic parameter to characterize the miscibility of polymers. The χ parameter involved in our simulation and introduced in eq 1 is a bare χ. In contrast, the χ parameter involved in SCFT calculations is an effective χ.

In the following, we consider only the case of symmetric polymers, i.e. with no difference in conformations. Within the framework of field-theoretic models, there are two main factors contributing to the difference between χ^b and χ^e: (i) local composition fluctuations, and (ii) the correlation−hole effect.[61,62] The latter effect arises because χ^e depend only the number of intermolecular interactions, not on the total number of interactions (i.e., intermolecular interactions do not contribute). References 58−60 have derived a relationship between the effective and bare χ's:

$$\chi^e = \chi^b \left[1 + \alpha \frac{l}{\lambda}\right]^{-1} \tag{8}$$

Here, l is the packing length, which in terms of our coarse-grained parameters is $R_e/\overline{N}$; λ is a cutoff-length and α is a numerical factor that depends on the approximation made ($\alpha = 18/\pi$ in ref 58 and $12/\pi$ in refs 59 and 60).

Finally, for models that are not field-theoretic, there is a third factor contributing to the difference between χ^b and χ^e, which is the local fluid-like structure induced on a length scale comparable to the monomer interaction range. While those packing effects are absent in the field-theoretic models where chains are represented as Gaussian threads with a vanishing interaction range, they are potentially significant in all particle-based models, such as systems of particles with pairwise interactions.

To assess the difference between χ^b and χ^e in the context of Monte Carlo simulations of the model considered in this work, we refer to Daoulas and Müller who examined the ratio of bare and effective system properties.[48] The diblock system considered in their work involved parameters ($\overline{N} = 122$, $\kappa N = 50$, $N = 32$, $\Delta L = 0.156R_e$) that are very close to those of the triblock systems considered here.The authors concluded that the differences do not amount to more than a few percent.

Also, note that for a different (grid-less) implementation of the Hamiltonian considered here, we have determined the difference between χ^b and χ^e. In that study,[53] each bead was assigned a density cloud and the nonbonded energy was expressed as a sum of pairwise interactions between beads. In that model, χ^b was the parameter entering the bead interaction potential and χ^e was estimated by using a mean-field equation of state. For the diblock system whose parameters are close to those of ref 48, it was found that $\chi^e = 0.82\chi^b$. We attribute that mismatch to packing effects induced by the pairwise interbead potential.[67]

■ ACKNOWLEDGMENT

This work was supported by the Semiconductor Research Corporation (SRC) and by the National Science Foundation (NSF). We are grateful to Marcus Müeller and Zheng-Gang Wang for helpful discussions.

REFERENCES

(1) Park, M.; Harrison, C.; Chaikin, P.; Register, R.; Adamson, D. *Science* **1997**, *276*, 1401.
(2) Bates, F.; Fredrickson, G. *Phys. Today* **1999**, *52*, 32.
(3) Stoykovich, M.; Kang, H.; Daoulas, K.; Liu, G.; Liu, C.; de Pablo, J.; Müller, M.; Nealey, P. *ACS Nano* **2007**, *1*, 168.
(4) Black, C. *ACS Nano* **2007**, *1*, 147.
(5) Black, C. *Nature* **2007**, *2*, 464.
(6) Urbas, A.; Maldovan, M.; DeRege, P.; Thomas, E. L. *Adv. Mater.* **2002**, *14*, 1850.
(7) Hillmyer, M. *Adv. Polym. Sci.* **2005**, *190*, 137.
(8) Hamley, I. *Nanotechnology* **2003**, *14*, 39.
(9) Li, M.; Conjarts, C.; Ober, C. *Adv. Polym. Sci.* **2005**, *190*, 183.
(10) Fasolka, M.; Mayes, A. *Annu. Rev. Mater. Res.* **2001**, *31*, 323.
(11) Kim, S.; Solak, H.; Stoykovich, M.; Ferrier, N.; de Pablo, J.; Nealey, P. *Nature* **2003**, *424*, 411.
(12) Edwards, E.; Montague, M.; Solak, H.; Hawker, C.; Nealey, P. *Adv. Mater.* **2004**, *16*, 1315.
(13) Ruiz, R.; Kang, H.; Detcheverry, F.; Dobisz, E.; Kercher, D.; Albrecht, T.; de Pablo, J.; Nealey, P. *Science* **2008**, *321*, 936.
(14) Hamley, I. *Prog. Polym. Sci.* **2009**in press.
(15) Ross, C.; Chaube, A. 2008.
(16) Cheng, J.; Rettner, C.; Sanders, D.; Kim, H.; Hinsberg, W. *Adv. Mater.* **2008**, *20*, 3155.
(17) Detcheverry, F.; Liu, G.; Nealey, P.; de Pablo, J. *Macromolecules* **2010**, *43*, 3446.
(18) Bates, F.; Schulz, M.; Khandpur, A.; Förster, S.; Rosedale, J.; Almdal, K.; Mortensen, K. *Faraday Discuss.* **1994**, *98*, 7.
(19) Khandpur, A.; Foerster, S.; Bates, F.; Hamley, I.; Ryan, A.; Bras, W.; Almdal, K.; Mortensen, K. *Macromolecules* **1995**, *28*, 8796.
(20) Knoll, A.; Lyakhova, K.; Horvat, A.; Krausch, G.; Sevnik, G.; Zvelindovsky, A.; Magerle, R. *Nanostructured Mater.* **2004**, *15*, 24.
(21) Knoll, A.; Horvat, A.; Lyakhova, K.; Krausch, G.; Sevink, G.; Zvelindovsky, A.; Magerle, R. *Phys. Rev. Lett.* **2002**, *89*, 35501.
(22) Zheng, W.; Wang, Z. *Macromolecules* **1995**, *28*, 7215.
(23) Matsen, M. W.; Schick, M. *Phys. Rev. Lett.* **1994**, *72*, 2660.
(24) Abetz, V.; Simon, P. *Adv. Polym. Sci.* **2005**, *189*, 125.
(25) Breiner, U.; Krappe, U.; Abetz, V.; Stadler, R. *Macromol. Chem. Phys.* **1997**, *198*, 1051.
(26) Breiner, U.; Krappe, U.; Jakob, T.; Abetz, V.; Stadler, R. *Polym. Bull.* **1998**, *40*, 219.
(27) Epps, T.; Bates, F. *Macromolecules* **2006**, *39*, 2676.
(28) Epps, T.; Cochran, E.; Bailey, T.; Waletzko, R.; Hardy, C.; Bates, F. *Macromolecules* **2004**, *37*, 8325.
(29) Epps, T.; Cochran, E.; Hardy, C.; Bailey, T.; Waletzko, R.; Bates, F. *Macromolecules* **2004**, *37*, 7085.
(30) Kikuchi, M.; Binder, K. *J. Chem. Phys.* **1994**, *101*, 3367.
(31) Wang, Q.; Yan, Q.; Nealey, P.; de Pablo, J. *Macromolecules* **2000**, *33*, 4512.
(32) Feng, J.; Ruckenstein, E. *Macromol. Theory Simul.* **2002**, *11*, 630.
(33) Huang, Y.; Liu, H.; Hit, Y. *Macromol. Theory Simul.* **2006**, *15*, 117.
(34) Nie, Z.; Su, Z.; Sun, Z.; Shi, T.; An, L. *Macromol. Theory Simul.* **2005**, *14*, 463.
(35) Kotelyanskii, M.; Th, K.; Theodorou, D. 2004.
(36) Binder, K. 1995.
(37) Bohbot-Raviv, Y.; Wang, Z. *Phys. Rev. Lett.* **2000**, *85*, 3428.
(38) Tang, P.; Qiu, F.; Zhang, H.; Yang, Y. *Phys. Rev. E* **2004**, *69*, 31803.
(39) Tang, P.; Qiu, F.; Zhang, H.; Yang, Y. *J. Phys. Chem. B* **2004**, *108*, 8434.
(40) Ye, X.; Yu, X.; Sun, Z.; An, L. *J. Phys. Chem. B* **2006**, *110*, 12042.
(41) Ye, X.; Shi, T.; Lu, Z.; Zhang, C.; Sun, Z.; An, L. *Macromolecules* **2005**, *38*, 8853.
(42) Guo, Z.; Zhang, G.; Qiu, F.; Zhang, H.; Yang, Y.; Shi, A. *Phys. Rev. Lett.* **2008**, *101*, 28301.
(43) Sun, M.; Wang, P.; Qiu, F.; Tang, P.; Zhang, H.; Yang, Y. *Phys. Rev. E* **2008**, *77*, 16701.
(44) Besold, G.; Hassager, O.; Mouritsen, O. *Comput. Phys. Commun.* **1999**, *121*, 542.
(45) Daoulas, K.; Müller, M.; Pablo, J.; Nealey, P.; Smith, G. *Soft Matter* **2006**, *2*, 573.
(46) Detcheverry, F.; Pike, D.; Nagpal, U.; Nealey, P.; Pablo, J. *Soft Matter* **2009**, *5*, 4858.
(47) Detcheverry, F.; Kang, H.; Daoulas, K.; Müller, M.; Nealey, P.; de Pablo, J. *Macromolecules* **2008**, *41*, 4989.
(48) Daoulas, K. C.; M. Müller, *J. Chem. Phys. 125*, 184904 (pages 18) (**2006**).
(49) Fredrickson, G. 2006.
(50) Helfand, E.; Tagami, Y. *J. Chem. Phys.* **1972**, *56*, 3592.
(51) Doi, M.; Edwards, S. 1988.
(52) Barrat, J.; Fredrickson, G.; Sides, S. *J. Phys. Chem. B* **2005**, *109*, 6694.
(53) Pike, D.; Detcheverry, F.; Müller, M.; de Pablo, J. *J. Chem. Phys.* **2009**, *131*, 084903.
(54) Wang, Q. *J. Chem. Phys.* **2008**, *129*, 054904.
(55) Chatterjee, J.; Jain, S.; Bates, F. *Macromolecules* **2007**, *40*, 2882.
(56) Stoykovich, M.; Müller, M.; Kim, S.; Solak, H.; Edwards, E.; de Pablo, J.; Nealey, P. *Science* **2005**, *308*, 1442.
(57) Müller, M.; Daoulas, K. *J. Chem. Phys.* **2008**, *128*, 024903.
(58) Wang, Z.-G. *J. Chem. Phys.* **2002**, *117*, 481.
(59) Olvera de la Cruz, M.; Edwards, S. F.; Sanchez, I. C. *J. Chem. Phys.* **1988**, *89*, 1704.
(60) Grzywacz, P.; Qin, J.; Morse, D. *Phys. Rev. E* **2007**, *76*, 1.
(61) Muller, M.; Binder, K. *Macromolecules* **1995**, *28*, 1825.
(62) Muller, M. *Macromol. Theory Simul.* **1999**, *8*, 343.
(63) In MC simulations, incompressibility would be obtained in the limit $\kappa N \rightarrow \infty$, but in practice, simulations become slow for $\kappa N > 10^3$.
(64) For other cases, the CSH morphology with end blocks forming the matrix has been predicted
(65) Here the point with $\Lambda = 0$. More details can be found in ref 17.
(66) Within the simulation time considered here. Much longer simulations, not accessible as of now, might yield a different result.
(67) In contrast to the gridless implementation, there is no obvious mechanism driving the local packing effects in the grid-based interaction employed here. Indeed beads interact only when located in the same cell, and, more importantly, the interaction does not depend on the position of the beads within the cell. As a consequence, we expect the packing effects to be very weak.